Electronic Supplementary Information for

Benzonitrile-Functionalized Non-Fullerene Acceptors for Organic Solar Cells with Low Non-Radiative Loss

Cheng-Zhe Sun, [a, †] *Xue Lai,* [b, †] *Tahir Rehman,* [b] *Hanjian Lai,* [b] *Chunxian Ke,* [b] *Xiangyu Shen,* [b] *Yulin Zhu,* [b] *Leilei Tian,* [*a] *and Feng He* [*b]

[a] Department of Materials Science and Engineering, Southern University of Science and Technology, Shenzhen, Guangdong 518055 (P. R. China)

E-mail: tianll@sustech.edu.cn

[b] Shenzhen Grubbs Institute, Guangdong Provincial Key Laboratory of Catalysis and Department of Chemistry, Southern University of Science and Technology, Shenzhen, Guangdong 518055 (P. R. China)

E-mail: hef@sustech.edu.cn

[†] These authors contributed equally to this work.

Characterization

^{1}H NMR spectra were recorded on Bruker AV 400 MHz spectrometer in deuterated chloroform solution at room temperature with tetramethylsilane (TMS) as the internal reference. ^{13}C NMR spectra were recorded on Bruker AV 600 MHz spectrometer in deuterated chloroform solution at room temperature with tetramethylsilane (TMS) as the internal reference. Cyclic voltammetry (CV) measurements were performed on a Model CHI 660E potentiostat/galvanostat (Shanghai Chenhua Industrial Co., Ltd. China) to determine the HOMO and LUMO levels of the acceptors, in an acetonitrile solution of 0.1 mol.L^{-1} tetrabutylammonium hexafluorophosphate ($[n\text{-}Bu_4N]^+[PF_6]^-$) at a potential scan rate of 100 mV s^{-1} with an Ag/Ag^+ reference electrode and a platinum wire counter electrode under an argon atmosphere. Thermogravimetric analysis (TGA) plots were measured with a Discovery series instrument under a nitrogen atmosphere at heating and cooling rates of 10 °C min^{-1}. UV-vis absorption spectra were recorded on a Shimadzu UV3600 spectrometer. High-resolution mass spectra were recorded on an Autoflex III matrix-assisted laser desorption ionization mass spectrometer (MALDI-TOF-MS). Atom force microscopy (AFM) images were taken on a NanoScopeIIIa controller (Veeco Metrology Group/Digital Instruments, Santa Barbara, CA), using built-in software (version V6.13R1) to capture images. Transmission electron microscopy (TEM) images were acquired using a TEM Hitachi H-7650 electron microscope operating at an acceleration voltage of 100 kV. Crystal data were collected on a Bruker D8 VENTURE diffractometer with graphite monochromated Cu Kα (λ = 1.54178).

Device Fabrication of Organic Solar Cells

Organic solar cells were fabricated on glass substrates commercially pre-coated with a layer of ITO with the conventional structure of ITO/PEDOT:PSS/D18:Acceptor/ PNDIT-F3N/Ag. The indium-tin-oxide (ITO) coated glass substrates were ultrasonicated sequentially in deionized water, acetone and isopropyl alcohol for 15 mins and dried in an oven at 80 °C. The ITO substrates were treated with UV-ozone for 15 mins and were spin-coated to get the neat PEDOT:PSS films. Then pre-annealing at

100 °C for 10 mins was performed. The corresponding active layer blend solutions (D18:Acceptor = 1:1.2, 11mg/ml, $CHCl_3$) were spin-coated at 3000 rpm for 30 s to form an active layer of 120 nm. Then an extra pre-annealing at 100 °C for 10 mins was performed. A 5 nm thick PNDIT-F3N film was deposited as the cathode buffer layer by the spin-coating of a solution of 0.5 mg/ml PNDIT-F3N in MeOH. Then the resulted active films were transferred into a vacuum chamber. A 10 nm MoO_3 and 100 nm Ag layer were subsequently evaporated through a shadow mask to define the active area of the devices. The integrated device structure is ITO/PEDOT:PSS/D18:Acceptor/PNDIT-F3N/Ag. A solar simulator (Enlitech Inc.) with an AM 1.5G filter was used as a light source to produce an intensity of 100 mW cm^{-2} for the illumination of the photovoltaic cell. The completed devices were tested in closed argon-filled glove box.

Characterization of Devices

The light intensity was calibrated by a 2 cm × 2 cm calibrated silicon solar cell with KG-3 visible color filter. A shadow mask with a single aperture (4.15 mm^2) was placed onto the devices in order to define the photoactive area accurately. The power conversion efficiencies (PCEs) were tested under this AM 1.5 G irradiation with the intensity of 100 mW cm^{-2} (Enlitech.Inc) which was calibrated by a NREL certified standard silicon cell (4 cm^{-2}). The J-V curves were recorded with the computer-controlled Keithley 2400 sourcemeter in a dry box under an inert atmosphere. The external quantum efficiency (EQE) spectra were measured through the measurement of solar cell spectral response measurement system QE-R3011 (Enli Technology Ltd.).

Electron-only and hole-only device fabrication

Electron-only devices were fabricated with the device structure of ITO/ZnO/D18:acceptor/PNDIT-F3N/Ag, while the hole-only devices were fabricated with the device structure of ITO/PEDOT:PSS/D18:acceptor/MoO_3/Ag. The mobilities were determined by fitting the dark current to the model of a single carrier SCLC,[1, 2] which is described by the equation:

$$J = \frac{9}{8}\varepsilon_0\varepsilon_r\mu_h\frac{V^2}{d^3}$$

Where J is current, μ_h is the zero-field mobility, ε_0 is the permittivity of free space, ε_r is the relative permittivity of the material, d is the thickness of the active layer and V is the effective voltage.

Energy Loss Investigation

Fourier transform photo-current spectroscopy external quantum efficiency (FTPS-EQE) and Electroluminescence (EL) were employed to investigate E_{loss} of these three CN acceptor devices (**Figure 3e**, **3f** and **Table 3**). According to Shockley-Queisser (SQ) limit,[3, 4] E_{loss} was defined by the following equations:

$$E_{loss} = E_g - qV_{OC} = \left(E_g - qV_{OC}^{SQ}\right) + \left(qV_{OC}^{SQ} - qV_{OC}^{rad}\right) + \left(qV_{OC}^{rad} - qV_{OC}\right) = \\ + q\Delta V_{OC}^{rad,\,below\,gap} + q\Delta V_{OC}^{non-rad} = \Delta E_1 + \Delta E_2 + \Delta E_3$$

Herein, ΔE_1 was the radiative recombination energy loss from the absorption above the optical bandgap, calculated by SQ theory. ΔE_2 was the radiative recombination energy loss from the absorption below the optical bandgap. ΔE_3 was the non-radiative energy loss. ΔE_3 and EQE_{EL} (EL quantum efficiency of OSCs) has one corresponding relationship as shown in the following equation

$$\Delta E_3 = -kTln(EQE_{EL})$$

Where k was the Boltzmann's constant and T was the absolute temperature.

Experimental Section

Materials

Compounds **1**, **3,** and **4** were synthesized according to the previously reported methods.[5-7] All the other chemicals were purchased as reagents grade from J&K, Energy, Macklin, Bide, and Sigma-Aldrich, and used without further purification.

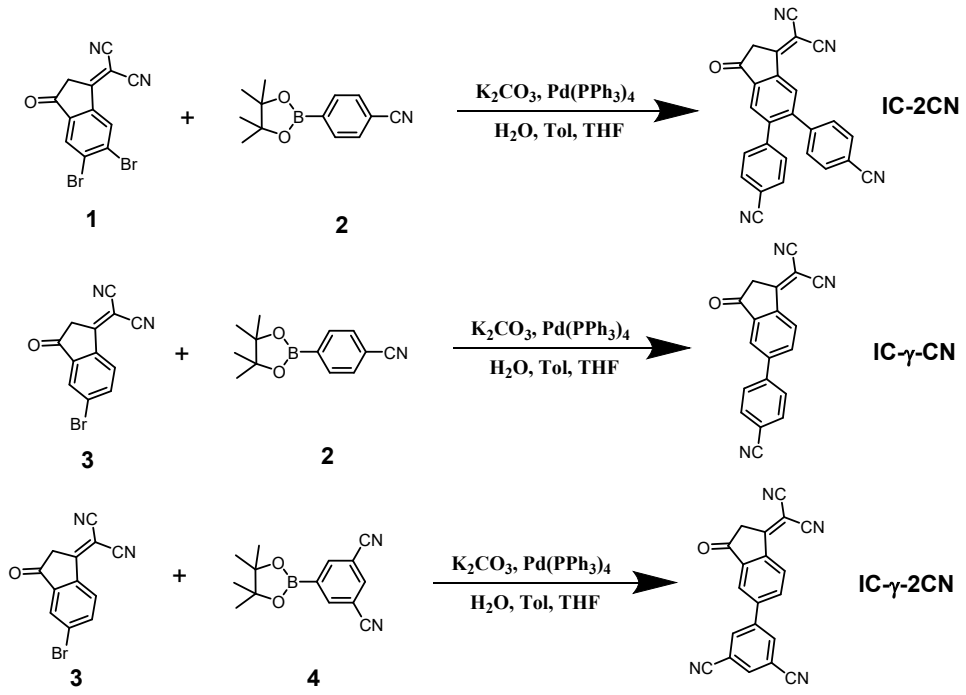

Figure S1. Synthetic routes of end group.

Synthesis of Compound IC-2CN

IC-2Br (290 mg, 0.824 mmol), 4-(4,4,5,5-tetramethyl-1,3,2-dioxaborolan-2-yl)benzonitrile (943 mg, 4.120 mmol), potassium carbonate (6.592 mmol, 910 mg), $Pd(PPh_3)_4$ (0.0165 mmol, 19 mg) and tetrahydrofuran(THF)/toluene/water (110ml, v/v/v = 3/2/0.5) were placed in a Schlenk tube under argon gas atmosphere, and refluxed for 24 hours. After cooling to room temperature, the mixture was poured into water (300 ml), which was extracted by ethyl acetate (100 ml) three times, and then washed with brine. The organic layer solution was collected and dried with anhydrous sodium sulfate. Then the solution was filtered and the solvent was removed under reduced pressure to give the crude product. The crude product was purified with silica-gel column chromatography with eluent (hexane/ethyl acetate/methanol = 10:1:0.5) to yield the pale-yellow solid (210 mg, 53.0%). ^{1}H NMR (400 MHz, Chloroform-*d*) δ 8.67 (s, 1H), 8.03 (s, 1H), 7.64 – 7.61 (m, 4H), 7.28 (s, 2H), 7.23 (s, 2H), 3.84 (s, 2H).

Synthesis of Compound IC-γ-CN

The same procedure as IC-2CN gave the desired pale-yellow solid product IC-γ-CN

(75.0%). ^{1}H NMR (400 MHz, Chloroform-*d*) δ 8.76 (dd, *J* = 8.4, 0.7 Hz, 1H), 8.18 (dd, *J* = 1.9, 0.7 Hz, 1H), 8.11 (dd, *J* = 8.4, 1.9 Hz, 1H), 7.84 (d, *J* = 8.7 Hz, 2H), 7.79 (d, *J* = 8.7 Hz, 2H), 3.80 (s, 2H).

Synthesis of Compound IC-γ-2CN

The same procedure as IC-2CN gave the desired pale-yellow solid product IC-γ-2CN (55.7%). ^{1}H NMR (400 MHz, Chloroform-*d*) δ 8.82 (d, *J* = 8.3 Hz, 1H), 8.16 (dd, *J* = 3.7, 1.6 Hz, 3H), 8.09 – 8.04 (m, 2H), 3.83 (s, 2H).

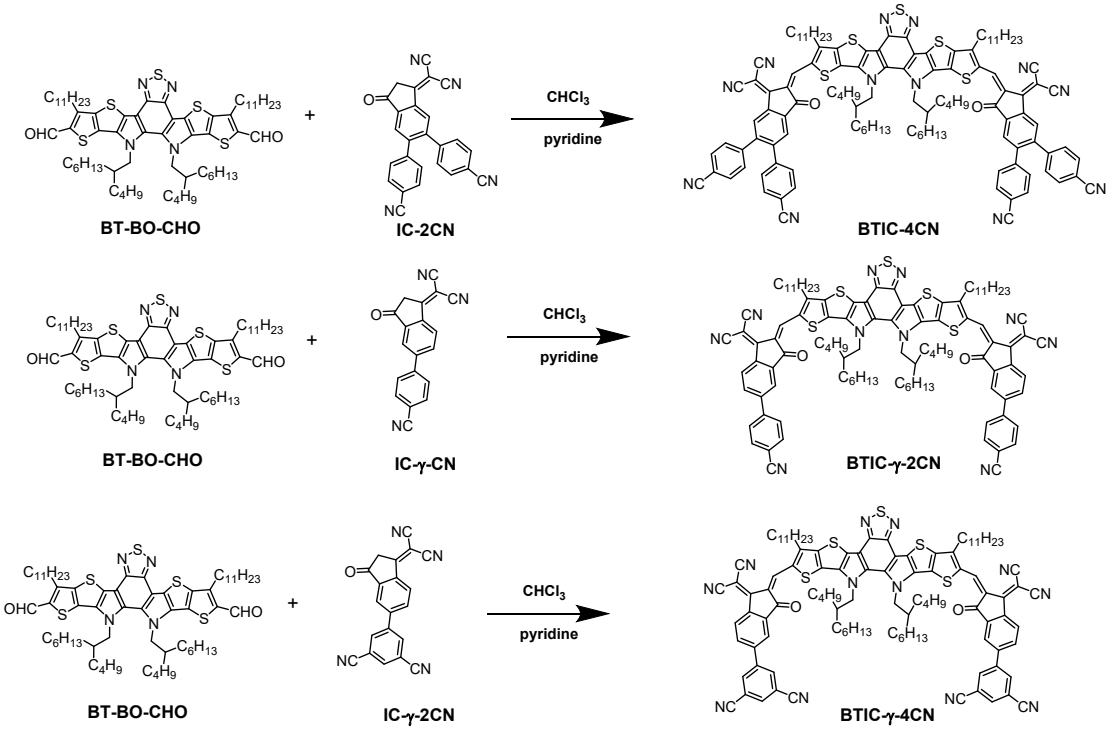

Figure S2. Synthetic routes of (a) **BTIC-4CN**, (b) **BTIC-γ-2CN**, (c) **BTIC-γ-4CN**.

Synthesis of BTIC-4CN

Compound BT-BO-CHO (62mg, 0.54mmol) and IC-4CN (238mg, 0.60mmol) were added into a 100 ml round bottom flask. After the flask was evacuated and backfill with argon gas three times, chloroform (50 ml) was added via a syringe immediately and then pyridine (1.0 ml) was added slowly. Then the mixture was refluxed at 70 °C for 24 hours. After cooling to room temperature, the product was precipitated in 250ml of methanol and then filtered. The crude product was purified through the column chromatography with chloroform as the eluent to yield the dark blue solid BTIC-4CN

(51 mg, 48.9%). ^{1}H NMR (400 MHz, Chloroform-*d*) δ 9.25 (s, 2H), 8.78 (d, *J* = 2.7 Hz, 2H), 7.97 (s, 2H), 7.63 (dd, *J* = 8.3, 3.2 Hz, 8H), 7.31 (d, *J* = 8.0 Hz, 8H), 4.76 (d, *J* = 8.0 Hz, 4H), 3.28 (t, *J* = 7.8 Hz, 4H), 2.14 (s, 2H), 1.96 – 1.87 (m, 4H), 1.39 (s, 4H), 1.26 (s, 27H), 1.09 (s, 12H), 1.02 – 0.90 (m, 16H), 0.89 – 0.83 (m, 9H), 0.65 (dq, *J* = 13.6, 7.1 Hz, 14H). ^{13}C NMR (151 MHz, Chloroform-*d*) δ 187.52, 153.91, 147.14, 145.30, 145.26, 144.67, 143.60, 143.49, 139.92, 137.89, 136.77, 136.05, 135.47, 133.83, 133.66, 132.52, 132.50, 130.57, 130.35, 130.27, 127.19, 125.34, 120.54, 118.10, 118.03, 115.12, 114.89, 113.74, 112.50, 55.78, 39.19, 31.92, 31.63, 31.26, 30.42, 29.99, 29.91, 29.72, 29.67, 29.63, 29.55, 29.35, 27.98, 27.88, 25.39, 22.89, 22.86, 22.69, 22.52, 22.51, 14.13, 14.05, 13.81, 13.79. HR-MS (MALDI-TOF) *m/z* calcd. for ($C_{118}H_{118}N_{12}O_2S_5$): 1895.814. Found: 1896.764.

Synthesis of BTIC-γ-2CN

The same procedure as BTIC-4CN gave the desired dark blue solid BTIC-γ-2CN (82.0%). ^{1}H NMR (400 MHz, Chloroform-*d*) δ 9.20 (s, 2H), 8.81 (d, *J* = 8.2 Hz, 2H), 8.15 (d, *J* = 1.8 Hz, 2H), 7.98 (d, *J* = 8.7 Hz, 2H), 7.88 – 7.79 (m, 8H), 4.78 (d, *J* = 7.9 Hz, 4H), 3.25 (t, *J* = 7.8 Hz, 4H), 2.16 (s, 2H), 1.89 (p, *J* = 8.0 Hz, 4H), 1.52 (t, *J* = 7.6 Hz, 4H), 1.38 (s, 4H), 1.25 (s, 32H), 1.10 (s, 5H), 1.03 – 0.93 (m, 12H), 0.86 (t, *J* = 6.7 Hz, 12H), 0.67 (dq, *J* = 14.1, 7.2 Hz, 13H). ^{13}C NMR (151 MHz, Chloroform-d) δ 187.96, 147.18, 145.09, 144.82, 139.78, 137.85, 135.75, 133.44, 133.10, 127.92, 125.82, 121.74, 118.37, 115.32, 114.90, 113.62, 112.93, 55.89, 39.26, 31.91, 31.64, 31.19, 30.52, 29.87, 29.84, 29.68, 29.63, 29.55, 29.34, 28.06, 27.96, 25.60, 22.95, 22.68, 22.55, 14.12, 14.09, 13.84. HR-MS (MALDI-TOF) *m/z* calcd. for ($C_{104}H_{112}N_{10}O_2S_5$): 1693.761. Found: 1693.923.

Synthesis of BTIC-γ-4CN

The same procedure as BTIC-4CN gave the desired dark blue solid BTIC-γ-4CN (78.43%). ^{1}H NMR (400 MHz, Chloroform-*d*) δ 9.23 (s, 2H), 8.87 (d, *J* = 8.2 Hz, 2H), 8.19 (d, *J* = 1.5 Hz, 4H), 8.09 (d, *J* = 1.9 Hz, 2H), 8.05 (t, *J* = 1.5 Hz, 2H), 7.95 (dd, *J* = 8.2, 1.9 Hz, 2H), 4.78 (d, *J* = 8.0 Hz, 4H), 3.27 (t, *J* = 7.9 Hz, 4H), 2.15 (s, 2H), 1.95

– 1.85 (m, 4H), 1.52 (d, *J* = 7.9 Hz, 4H), 1.38 (s, 4H), 1.26 (s, 30H), 1.10 (s, 8H), 0.98 (dd, *J* = 14.1, 6.9 Hz, 13H), 0.89 – 0.83 (m, 9H), 0.73 – 0.60 (m, 14H). ^{13}C NMR (151 MHz, Chloroform-*d*) δ 187.51, 153.86, 147.21, 145.26, 142.00, 141.70, 140.52, 138.02, 137.85, 136.12, 135.51, 135.00, 134.45, 133.88, 133.63, 133.24, 126.19, 121.61, 116.21, 115.39, 115.19, 114.81, 113.72, 55.86, 39.25, 31.91, 31.63, 31.26, 29.89, 29.67, 29.62, 29.53, 29.34, 28.05, 27.94, 22.89, 22.68, 22.53, 22.52, 14.12, 14.10, 14.09, 13.84, 13.82. HR-MS (MALDI-TOF) *m/z* calcd. for ($C_{106}H_{110}N_{12}O_2S_5$): 1743.751. Found: 1743.827.

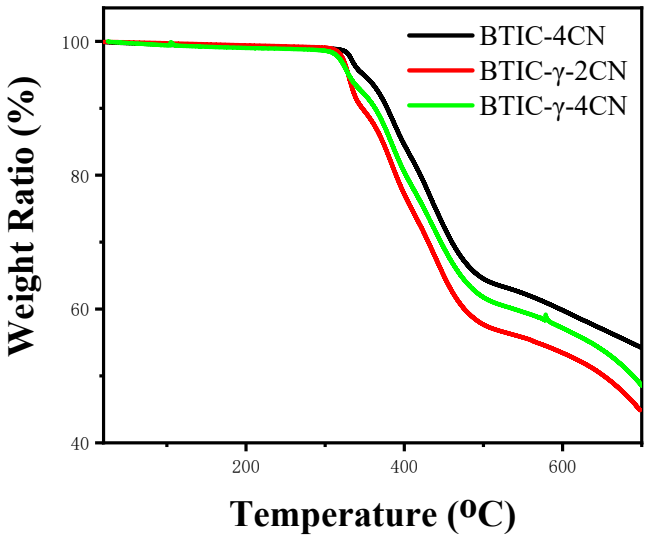

Figure S3. Thermogravimetric curves of BTIC-4CN, BTIC-γ-2CN, and BTIC-γ-4CN at a heating/cooling rate of 10 °C min^{-1} in N_2.

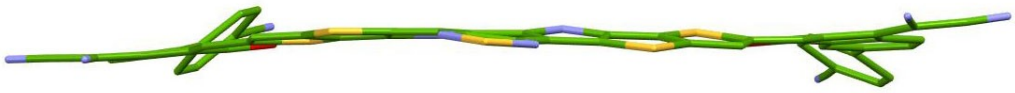

Figure S4. Side view of BTIC-γ-2CN Single crystal structure.

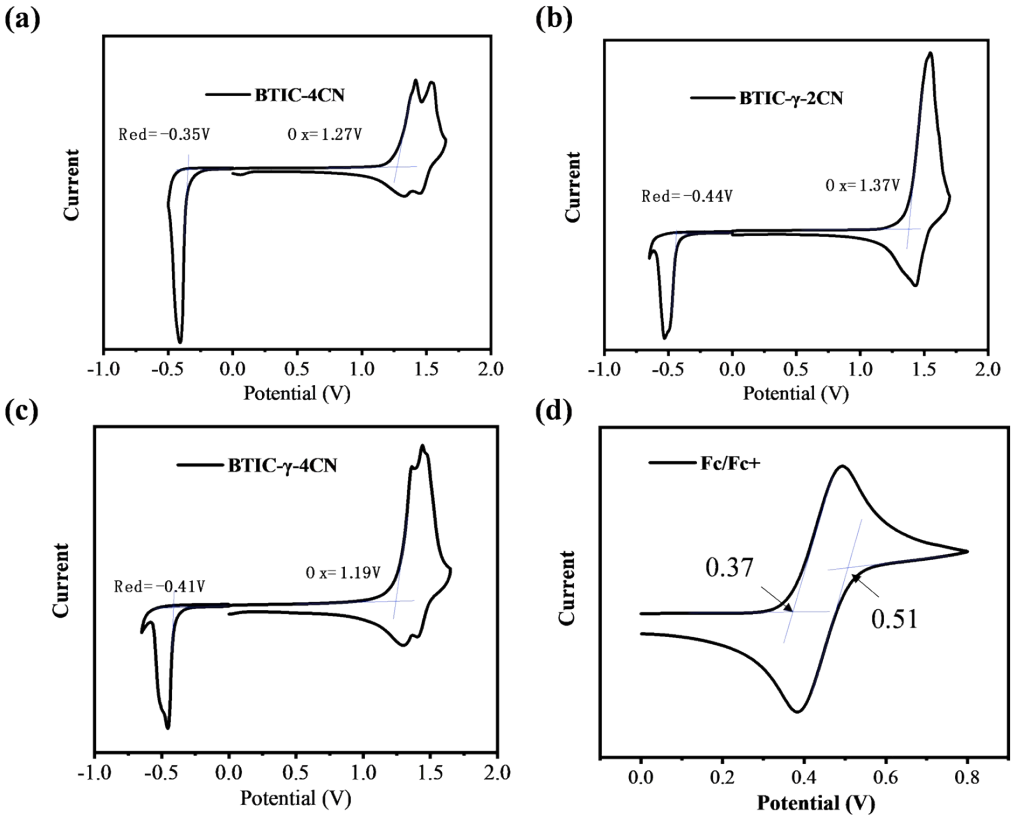

Figure S5. Cyclic voltammograms of three NFAs and Fc/Fc^+ in acetonitrile with (n-Bu)$_4NPF_6$ (0.1 M) as supporting electrolyte, Pt wire as a counter electrode, and Ag/Ag^+ as a reference electrode.

According to the equation of $E_{HOMO/LUMO} = -e(\varphi_{ox/red} + 4.8 - \varphi_{Fc/Fc+})$, the frontier energy levels and electrochemical bandgap (E_g^{cv}) of the acceptors are calculated as follows:

For **BTIC-4CN**: $E_{HOMO} = -e(1.27 + 4.8 - 0.44) = -5.63\ eV$;

$E_{LUMO} = -e(-0.35 + 4.8 - 0.44) = -4.01\ eV$;

$E_g^{cv} = E_{LUMO} - E_{HOMO} = 1.62\ eV$.

For **BTIC-γ-2CN**: $E_{HOMO} = -e(1.37 + 4.8 - 0.44) = -5.73\ eV$;

$E_{LUMO} = -e(-0.44 + 4.8 - 0.44) = -3.92\ eV$;

$E_g^{cv} = E_{LUMO} - E_{HOMO} = 1.81\ eV$.

For **BTIC-γ-4CN**: $E_{HOMO} = -e(1.19 + 4.8 - 0.44) = -5.55\ eV$;

$E_{LUMO} = -e(-0.41 + 4.8 - 0.44) = -3.95\ eV$;

$E_g^{cv} = E_{LUMO} - E_{HOMO} = 1.60\ eV$.

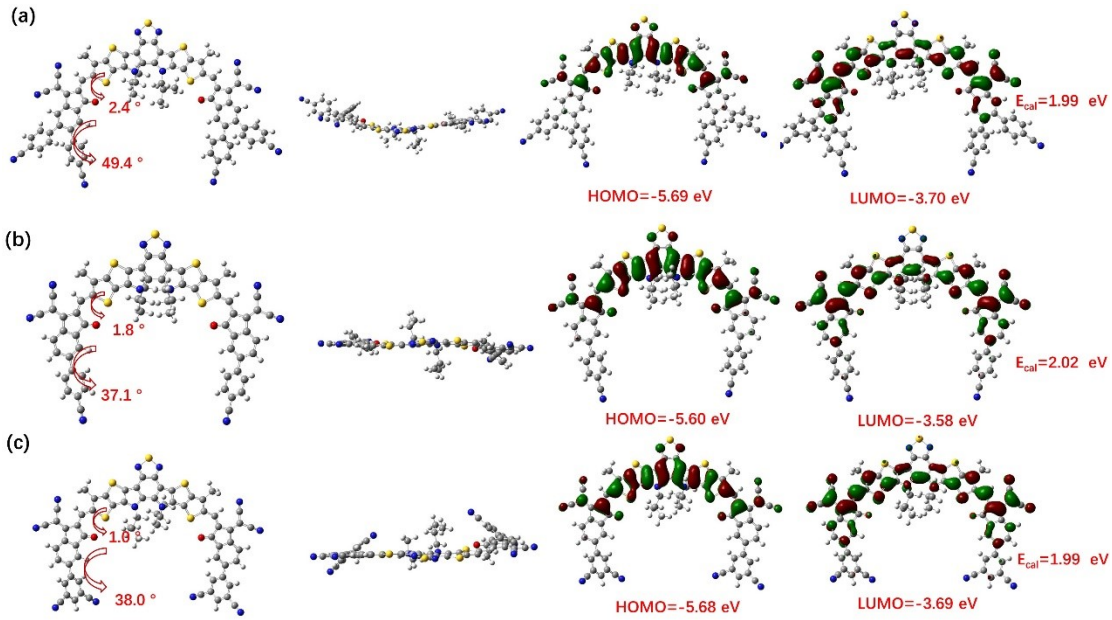

Figure S6. The DFT calculation (Optimized geometries, side view and calculated molecular orbitals) of (a) BTIC-4CN, (b) BTIC-γ-2CN and (c) BTIC-γ-4CN molecules.

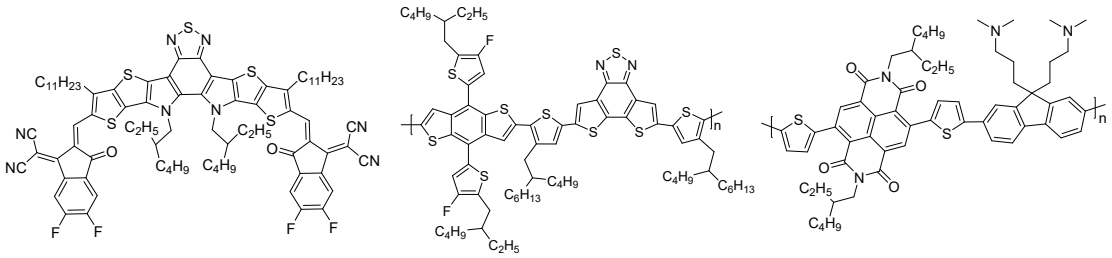

Figure S7. The molecular structures of Y6, D18 and PNDIT-F3N.

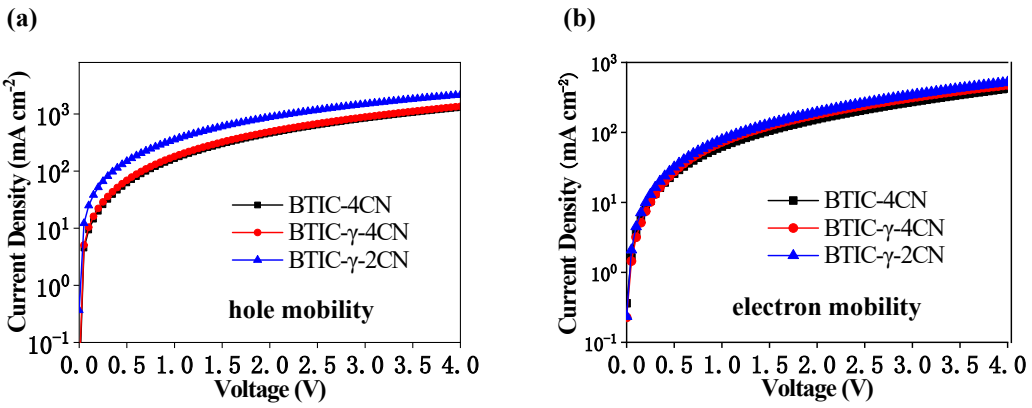

Figure S8. (a) The hole mobility curves, (b) the electron mobility curves.

Table S1. The SCLC mobility data for the blend of each acceptor.

Acceptors	Hole mobility μ_h (10^{-4} cm^2 V^{-1} s^{-1})	Electron mobility μ_e (10^{-4} cm^2 V^{-1} s^{-1})	Hole/Electron μ_h/μ_e
BTIC-4CN	4.1	1.5	2.7
BTIC-γ-2CN	8.7	1.9	4.6
BTIC-γ-4CN	4.4	1.8	2.4

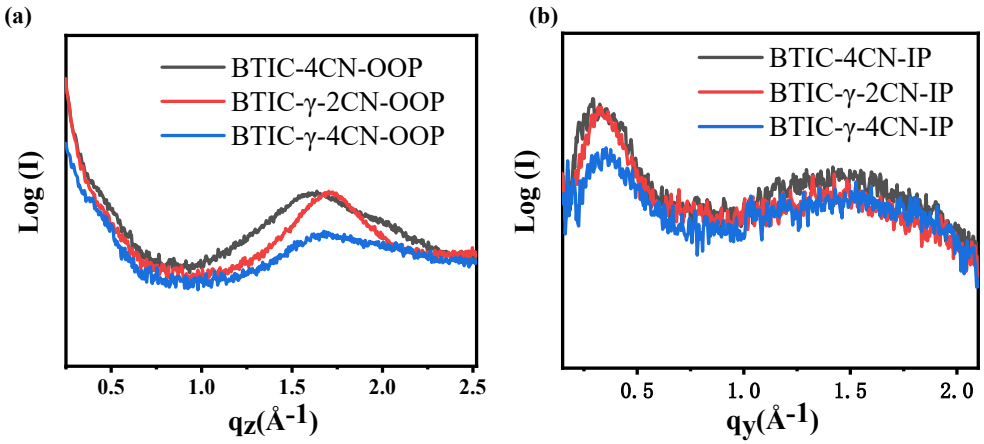

Figure S9. GIWAXS line cuts of the (a) out of the plane and (b) in-plane among the neat films.

Table S2. GIWAXS π-π stacking and lamellar peaks and distances in neat film

neat film	(010) π-π stacking		(100) lamellar	
	peak (Å^{-1})	distance (Å)	peak (Å^{-1})	distance (Å)
BTIC-4CN	1.636	3.84	0.292	21.52
BTIC-γ-2CN	1.703	3.63	0.332	18.92
BTIC-γ-4CN	1.687	3.72	0.339	18.53

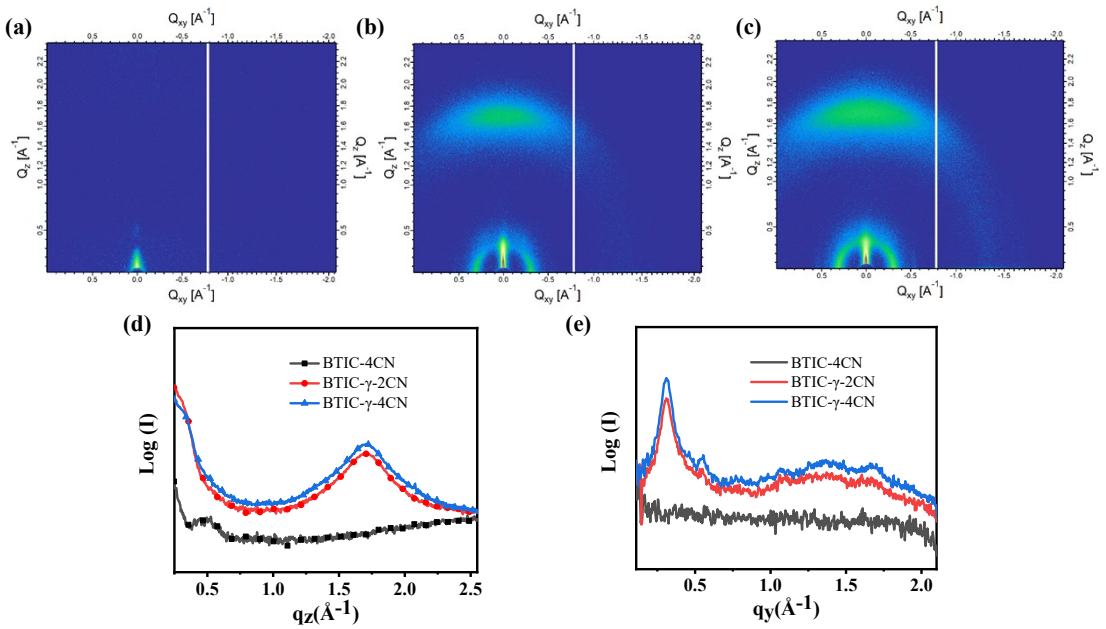

Figure S10. 2D GIWAXS images of (a) D18:BTIC-4CN blend film, (b) D18:BTIC-γ-2CN blend film and (c) D18:BTIC-γ-4CN blend film. GIWAXS line cuts of the (d) out of plane and (e) in-plane among the blend films.

Table S3. Detailed photovoltaic parameters of the Y6:BTIC-γ-2CN based ternary OSCs device

Donor	BTIC-γ-2CN (wt%)	J_{SC} (mA m^{-2})	V_{OC} (V)	FF (%)	PCE_{max} (%)	$J_{SC,EQE}$ (mA/cm^{-2})
D18	0	25.29	0.867	77.08	16.90	25.30
	5%	25.15	0.879	78.07	17.26	24.94
	10%	25.27	0.882	79.14	17.61	25.20
	20%	25.38	0.883	77.22	17.30	25.11
	30%	24.74	0.893	76.84	17.22	24.93
	100%	22.54	0.926	76.76	16.03	21.83

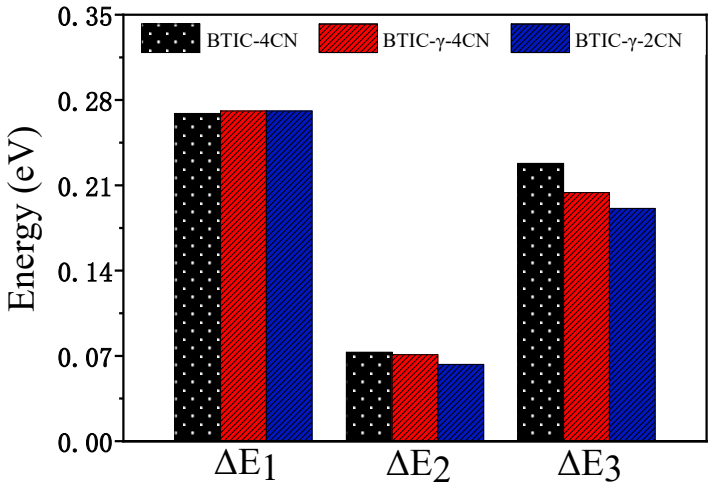

Figure S11. Energy loss of the acceptor-based devices.

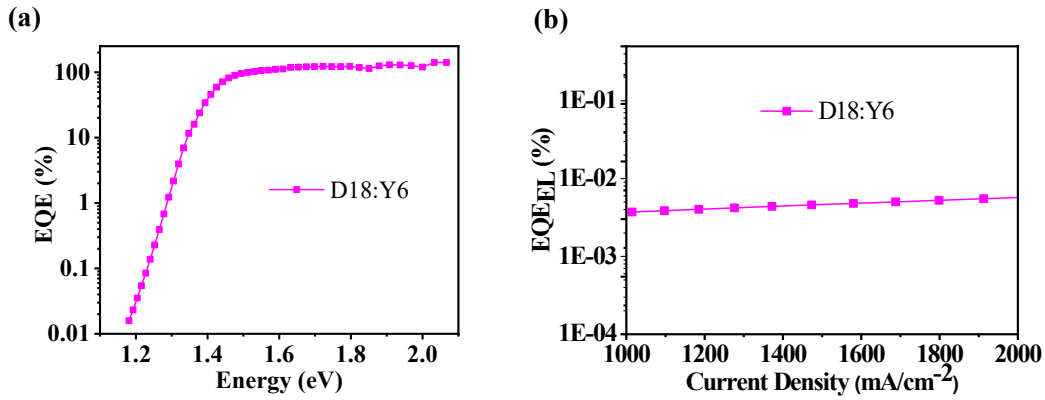

Figure S12. (a) EQE vs. energy curves and (b) EQE_{EL} curves of D18:Y6 based devices.

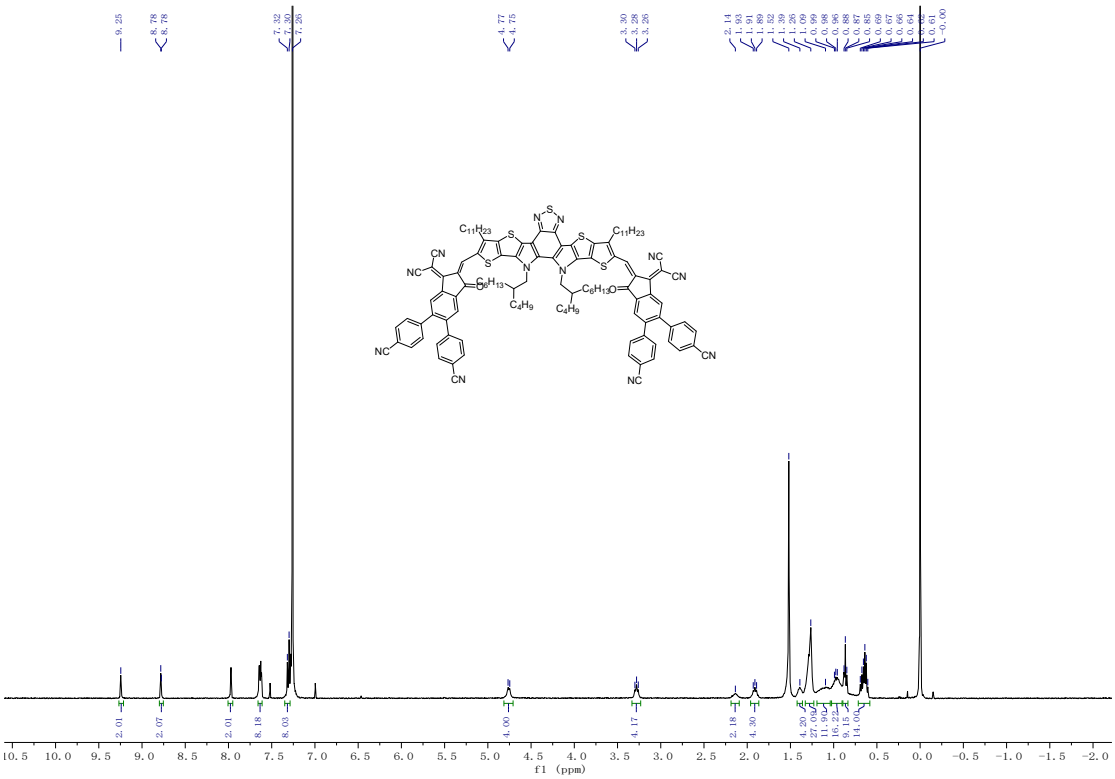

Figure S13. ^{1}H NMR of BTIC-4CN in $CDCl_3$.

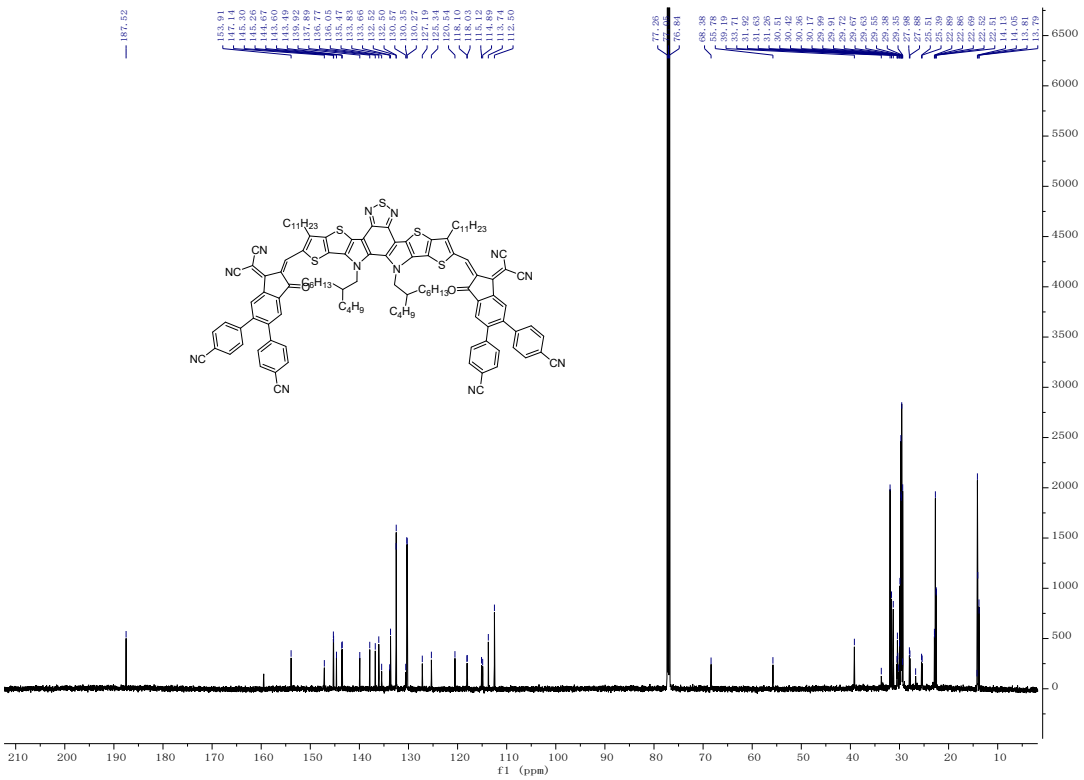

Figure S14. ^{13}C NMR of BTIC-4CN in $CDCl_3$.

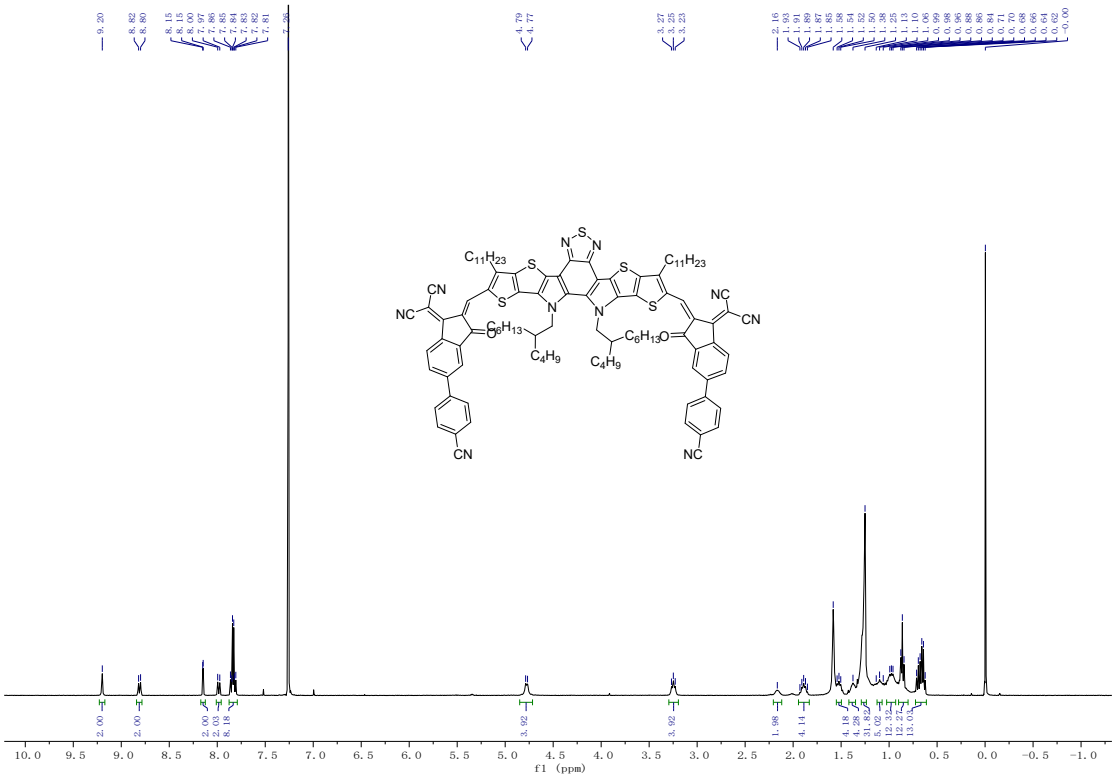

Figure S15. ^{1}H NMR of BTIC-γ-2CN in $CDCl_3$.

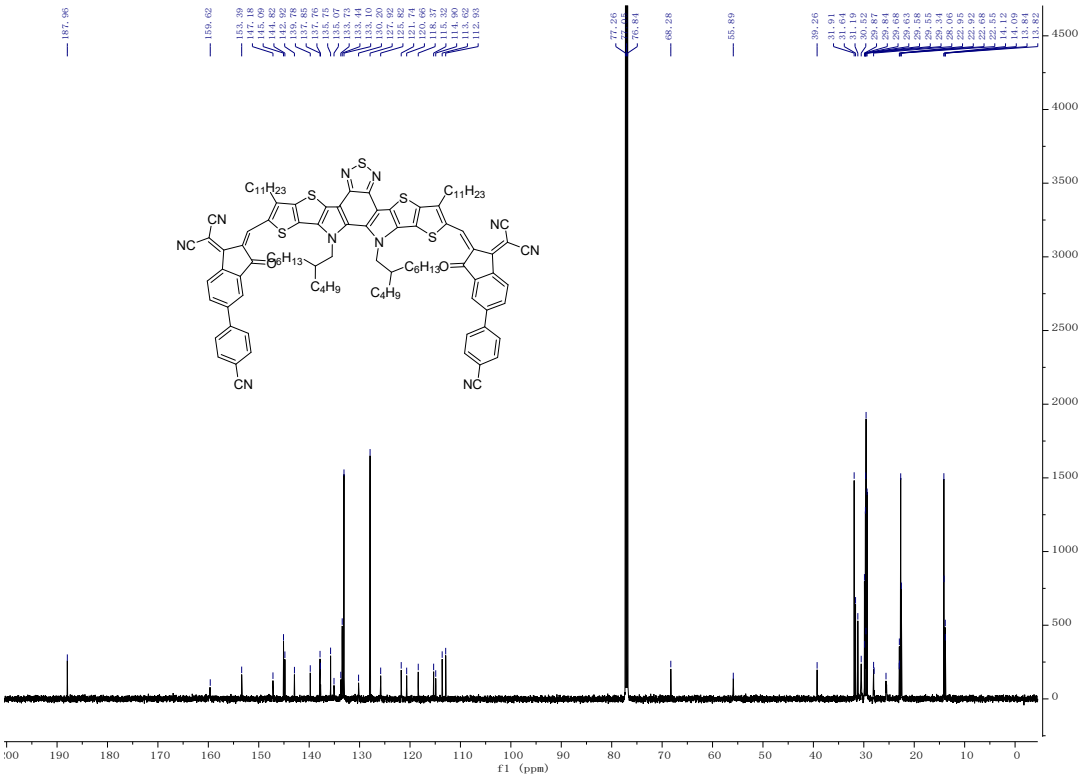

Figure S16. ^{13}C NMR of BTIC-γ-2CN in $CDCl_3$.

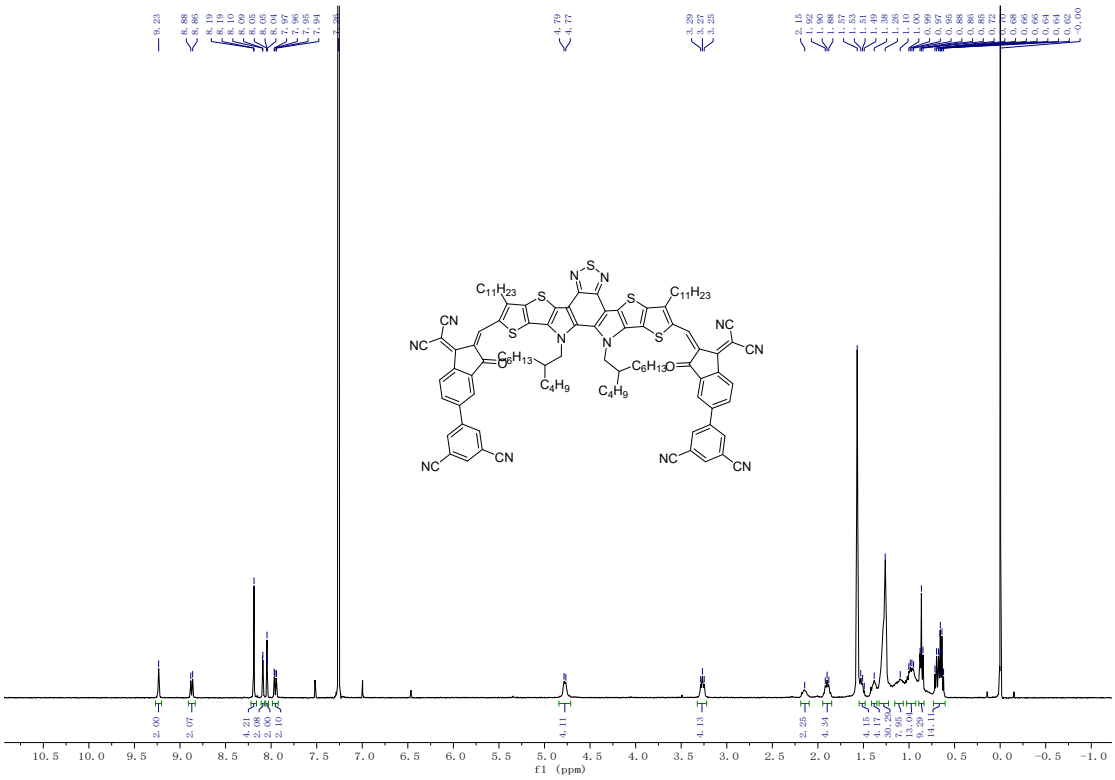

Figure S17. ^{1}H NMR of BTIC-γ-4CN in $CDCl_3$.

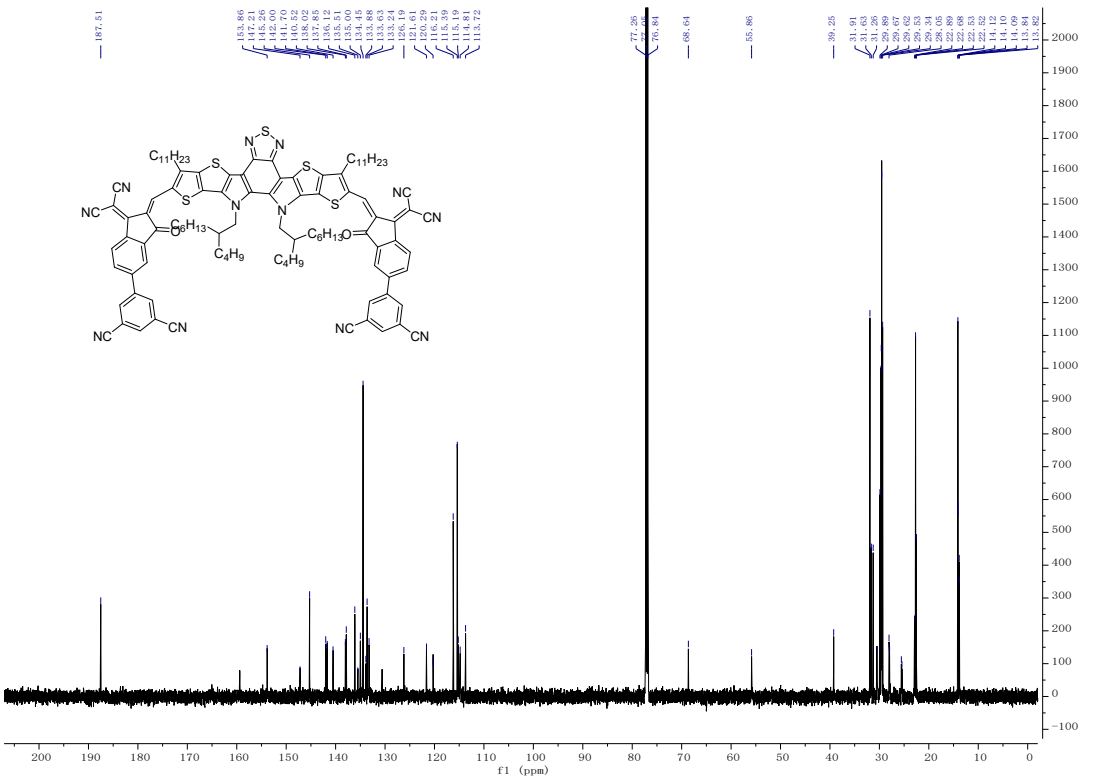

Figure S18. ^{13}C NMR of BTIC-γ-4CN in $CDCl_3$.

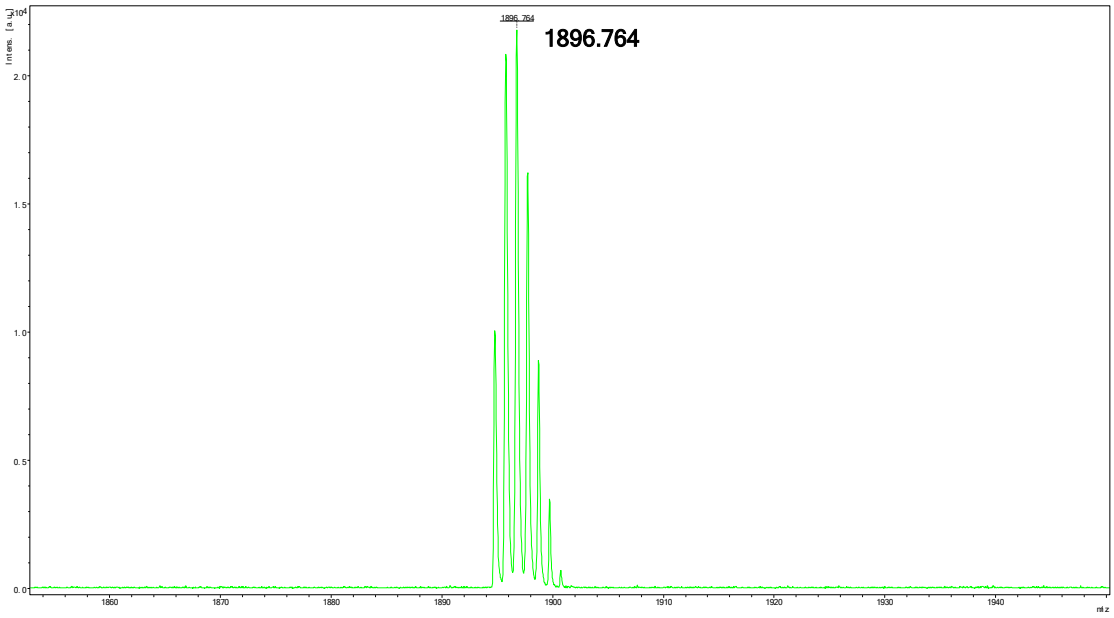

Figure S19. MS-MALDI spectrum of BTIC-4CN.

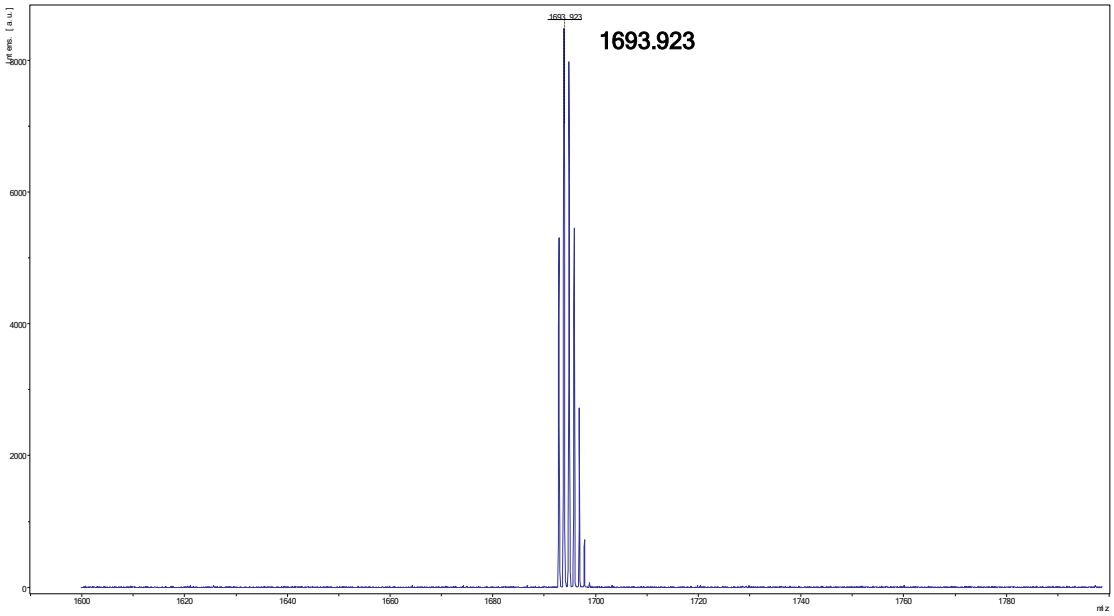

Figure S20. MS-MALDI spectrum of BTIC-γ-2CN.

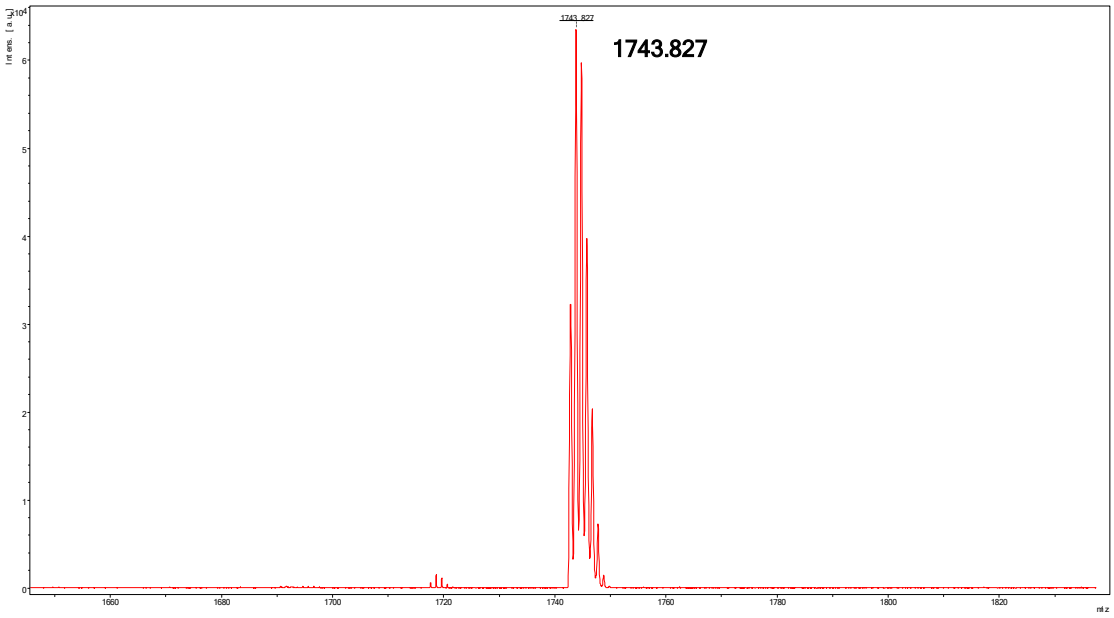

Figure S21. MS-MALDI spectrum of BTIC-γ-4CN.

References

1. P. S. Davids, I. H. Campbell and D. L. Smith, *J. Appl.Phys.*, 1997, **82**, 6319-6325.
2. V. D. Mihailetchi, J. Wildeman and P. W. M. Blom, *Phys.Rev. Lett.*, 2005, **94**, 126602.
3. W. Shockley and H. J. Queisser, *J. Appl.Phys.*, 1961, **32**, 510-519.
4. Y. Wang, D. Qian, Y. Cui, H. Zhang, J. Hou, K. Vandewal, T. Kirchartz and F. Gao, *Adv. Energy Mater.*, 2018, **8**, 1801352.
5. D. Mo, H. Chen, Y. Zhu, H.-H. Huang, P. Chao and F. He, *ACS Appl. Mater. Inter.*, 2021, **13**, 6147-6155.
6. H. Wang, H. Chen, W. Xie, H. Lai, T. Zhao, Y. Zhu, L. Chen, C. Ke, N. Zheng and F. He, *Adv. Funct. Mater.*, 2021, **31**, 2100877.
7. L.-A. Fendt, H. Fang, M. E. Plonska-Brzezinska, S. Zhang, F. Cheng, C. Braun, L. Echegoyen and F. Diederich, *Eur. J. Org. Chem.*, 2007, **2007**, 4659-4673.